

Wind gusts and plant aeroelasticity effects on the aerodynamics of pollen shedding: a hypothetical turbulence-initiated wind-pollination mechanism

Javier Urzay^a, Stefan G. Llewellyn Smith^a, Elinor Thompson^b, Beverley J. Glover^b

^a*Department of Mechanical and Aerospace Engineering, Jacobs School of Engineering, University of California San Diego, 9500 Gilman Drive, La Jolla, California 92093-0411, USA*

^b*Department of Plant Sciences, University of Cambridge, Downing Street, Cambridge CB2 3EA, UK*

Abstract

Plant reproduction depends on pollen dispersal. For anemophilous (wind-pollinated) species, such as grasses and many trees, shedding pollen from the anther must be accomplished by physical mechanisms. The unknown nature of this process has led to its description as the ‘paradox of pollen liberation’. A simple scaling analysis, supported by experimental measurements on typical wind-pollinated plant species, is used to estimate the suitability of previous resolutions of this paradox based on wind-gust aerodynamic models of fungal-spore liberation. According to this scaling analysis, the steady Stokes drag force is found to be large enough to liberate anemophilous pollen grains, and unsteady boundary-layer forces produced by wind gusts are found to be mostly ineffective since the ratio of the characteristic viscous time scale to the inertial time scale of acceleration of the wind stream is a small parameter for typical anemophilous species. A hypothetical model of a stochastic aeroelastic mechanism, initiated by the atmospheric turbulence typical of the micrometeorological conditions in the vicinity of the plant, is proposed to contribute to wind pollination.

Key words: Aeroelasticity, Wind Pollination, Pollen Aerodynamics, Plant Biomechanics

1. Introduction

All land plants are descended from a single lineage that made the transition from water to land approximately 470 million years ago. Perhaps the biggest challenge of adaptation to life on land was that of reproduction without the benefit of a surrounding aqueous environment for gamete dispersal. It was not until the origins of the seed plants, around 300 million years ago, that plants freed themselves from the need for external water for reproduction, by means of desiccation-resistant pollen and protected ovules retained within the parental tissue (Willis and McElwain, 2002). The pollen grain can be thought of as a waterproof dispersal vehicle containing the male gametes and associated cells. The success of the land plants was dependent upon the effectiveness of these dispersal vehicles. The first seed plants were wind pollinated, and wind pollination has remained the norm for the majority of gymnosperm lineages, which dominate ecosystems such as the Arctic and Siberian tundra. The first angiosperms are believed to have been insect-pollinated (Crane et al., 1995), but a large proportion of angiosperm species (around 25,000, or 10% of the total) evolved wind pollination secondarily (Willis and McElwain, 2002). These species include the ecologically dominant grasses, whose pollen is responsible for many human allergic

reactions, and whose successful pollination is essential to the production of cereal crops.

At pollen maturity, the thecae of the anthers dehydrate and split open as shown in Figure 1, leaving the pollen grains exposed to the ambient air flow and subject to a set of environmental forces. This ultimately leads to the pollen’s removal if the external forces overcome the threshold imposed by molecular adhesion. Accomplishing this loss without the aid of animals is no easy task for anemophilous pollen, which leads, by extension of the functionally similar process of fungal spore liberation (Aylor, 1975; Aylor and Parlange, 1975; Aylor, 1999), to the ‘paradox of pollen liberation’ (Jackson and Lyford, 1999), according to which the wind speed necessary to detach pollen and small fungal spores, as predicted by steady aerodynamic theory, is much larger than the threshold wind speed measured in the field.

The release, dispersal and deposition of pollen grains has been extensively reviewed (Niklas, 1985) but, contrary to the case of fungal-spore liberation (Aylor, 1975; Aylor and Parlange, 1975; Aylor, 1999), the fundamental problem of pollen liberation has not been resolved. We return to this problem using scaling analysis to clarify the conditions under which classical spore-removal descriptions (Aylor, 1975; Aylor and Parlange, 1975; Aylor, 1999) are appropriate to describe pollen shedding, and then propose a new model that explicitly takes into account both the turbulent nature of the micrometeorological conditions in the vicinity of the plant and the elastic and aerodynamic properties of the plant.

Email addresses: jurzay@ucsd.edu (Javier Urzay), sgls@ucsd.edu (Stefan G. Llewellyn Smith), et250@cam.ac.uk (Elinor Thompson), bjg26@cam.ac.uk (Beverley J. Glover)

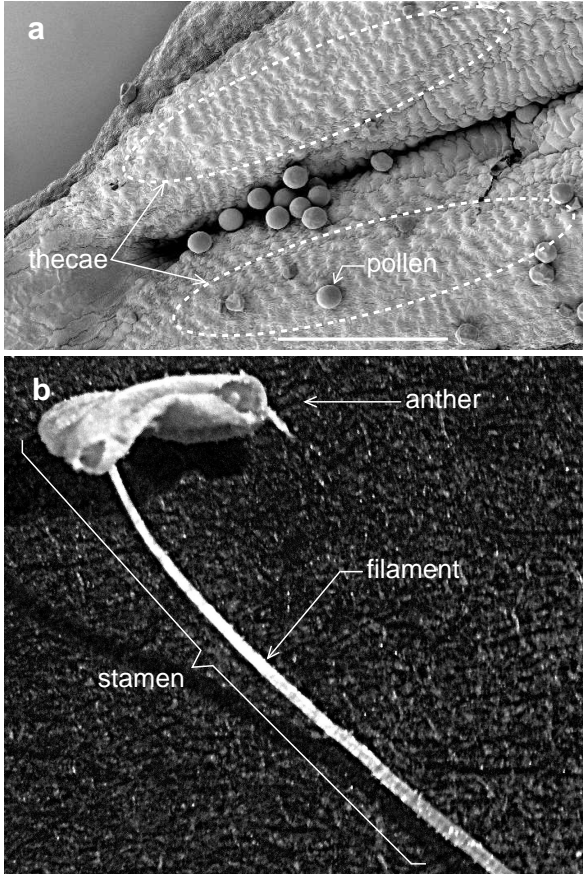


Figure 1: a) *Plantago* anther showing the thecae and the exposed pollen grains during dehiscence (scale bar 200 μm). b) *Plantago* stamen.

2. Aerodynamic shedding forces in boundary-layer air-flow models.

2.1. Steady aerodynamic forces.

Earlier analyses of the physical processes involved in pollen and small fungal spore liberation are based on boundary-layer air flow models around a pollen grain on an anther (Aylor, 1975; Aylor and Parlange, 1975; Niklas, 1985; Jackson and Lyford, 1999; Aylor, 1999), as depicted in Fig. 2. The pollen grain is assumed to be a spherical particle of equivalent diameter D and mass m_p . Wind-pollinated pollen grains are mostly of similar sizes, and tend to be round and smooth. Their exact shape can be shown to have only a small influence in the low-speed flow regimes encountered in the classic steady aerodynamic explanations of release since the drag force is mainly dominated by the skin (shear-stress) drag, and is of no importance in the stochastic aeroelastic mechanism proposed in section 3. We develop here a scaling analysis, supported by experimental measurements on typical wind-pollinated species (see Appendix A, Table 1), to analyze the effect of aerodynamic forces experienced by the pollen grain on an anther. The relative importance of inertial and viscous forces in a fluid is expressed as a dimensionless number, the Reynolds number $\text{Re}_L = UL/\nu$, where U is the fluid velocity, L is a characteristic length and $\nu = \mu/\rho$ is the kinematic viscosity, with μ and ρ respectively the dy-

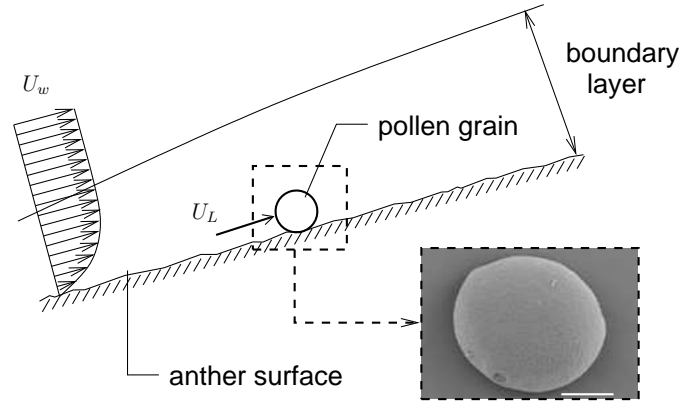


Figure 2: The boundary-layer model. The inset shows a *Betula albosinensis* pollen grain (scanning electron microscopy, scale bar 10 μm .)

namic viscosity and density of the fluid, which in the present analysis correspond to the viscosity and density of the air at standard conditions: $\mu = 1.85 \cdot 10^{-5}$ Pa-s, $\rho = 1.18$ kg/m³ and $\nu = 1.57 \cdot 10^{-5}$ m²/s.

The steady air flow around a typical anther of length $L \sim 0.6 - 4.3$ mm (see Table 1) is a laminar boundary-layer flow, resulting in $\text{Re}_L = U_w L/\nu \sim 36 - 271$ at ordinary wind speeds $U_w \sim 1$ m/s. Using boundary-layer scaling (Schlichting, 1979), a typical pollen grain of diameter $D \sim 16.7 - 95.3$ μm (see Table 1) is affected by local wind speeds U_L^∞ of order

$$U_L^\infty \sim 0.166 U_w \text{Re}_L^{1/2} D/L, \quad (1)$$

where the superindex $^\infty$ denotes its steady value. In this formulation, since the pollen grain is well embedded in the boundary layer, $D/2L \ll 1/\text{Re}_L^{1/2}$, use has been made of the well-known boundary-layer theory result that the friction coefficient on the anther surface is given by $0.664/\text{Re}_L^{1/2}$ (Schlichting, 1979), from which the local shear flow can be linearized and the local velocity is obtained as (1). The local velocity ranges in the interval $U_L^\infty \sim 18.0 - 40.7$ mm/s, resulting in local Reynolds numbers $\text{Re}_D = U_L^\infty D/\nu \sim 0.03 - 0.13$: the flow is essentially fully viscous at scales of order D . The disparity between the free-stream wind speed, U_w , and that close to the anther, U_L , is inherent in boundary-layer flows because of viscosity, and is the reason why steady aerodynamic forces are not sufficient to remove small fungal spores under steady aerodynamic conditions for typical wind speeds (Aylor, 1975; Aylor and Parlange, 1975; Jackson and Lyford, 1999; Aylor, 1999). The steady Stokes drag force on a spherical particle of the same size as a pollen grain in contact with a planar wall (O'Neill, 1999) is

$$F_D^\infty = 1.7009 \cdot (3\pi\mu D U_L^\infty), \quad (2)$$

giving $F_D^\infty \sim 0.1 - 0.6$ nN for the species analyzed in Table 1 and $U_w = 1$ m/s, and $F_D^\infty = 3.9 - 19.7$ nN for $U_w = 10$ m/s. The exact value of the adhesion force F_{ad} is poorly known, but reported measurements range from 0.1 - 1 nN for insect-pollinated species (King and Lengoc, 1993; King and Buchmann, 1999) to 100 nN for fungal spores (Aylor and Parlange, 1975). According to these estimates, the steady

Stokes aerodynamic drag F_D^∞ may in fact be large enough to shed typical pollen grains during steady wind conditions, since anemophilous pollen-anther adhesion forces F_{ad} are expected to be reasonably smaller than the upper-limit values of 0.1 – 1 nN for insect-pollinated species (King and Lengoc, 1993; King and Buchmann, 1999), which have a sticky layer of pollenkitt absent from the surface of anemophilous pollen grains.

2.2. Unsteady aerodynamic forces.

To solve a functionally similar paradox, that of fungal spores liberation from infected plant leaves, earlier work on conidia of *Helminthosporium maydis* (*Cochliobolus heterostrophus*; Southern corn leaf blight), 96 μm in length and 17 μm in diameter, 75 nN adhesion force, (Aylor, 1975; Aylor and Parlange, 1975) proposed the existence of gusts of wind with velocity fluctuations $u' = 2.5\text{m/s}$ that take place over a small distance, which corresponds to the gust front thickness $\delta_o = 1\text{mm}$, so that at a fixed point on the leaf the velocity fluctuation u' is swept over that point in a time of order

$$t_o = \delta_o / u' \sim 0.4 \text{ ms}, \quad (3)$$

causing the removal of spores by unsteady aerodynamic forces. The existence of wind gusts is consistent with subsequent analyses of canopy turbulence (Aylor, 1999; Finnigan, 2000; De Langre, 2008): the turbulence in the canopy of trees or smaller plants displays striking differences to classical turbulent boundary layers in that a mixing-layer instability and the canopy-induced internal wakes may trigger severe intermittency and wind gusts in the canopy region.

Atmospheric conditions typical of instability are also found during pollen release (Jackson and Lyford, 1999). However, when the same wind-gust explanation is applied to describe pollen shedding, the resulting unsteady forces exerted by the surrounding air on the pollen grain may not lead to pollen release, since the viscous time scale

$$t_v = D^2 / \nu \sim 0.02 - 0.58 \text{ ms}, \quad (4)$$

is typically the smallest time scale of the problem as observed in Appendix A, Table 1, where typical values of the viscous to wind-gust time scale ratio (i.e. the Stokes-Reynolds number)

$$\epsilon = t_v / t_o, \quad (5)$$

are listed for typical wind-pollinated species. Assuming (3) as a typical value of wind-gust time scale, ϵ is found to be a small parameter, $\epsilon \ll 1$, for most of the species listed in Table 1. There may be exceptions to this rule, such as maize pollen, for which gravitational force may also play a role in pollen removal because of its heavy weight.

It must be emphasized that, contrary to some fungal spores, which are liberated from conidiophores that extend higher into the boundary layer (Aylor, 1975; Aylor and Parlange, 1975; Aylor, 1999), pollen grains are mostly liberated directly from the anther surface, so that removal by wind gusts may not be so effective for them as detailed below.

Figure 3a shows a frozen sketch of the flow field around a pollen grain, after times of order t_o , for the hypothetical case of

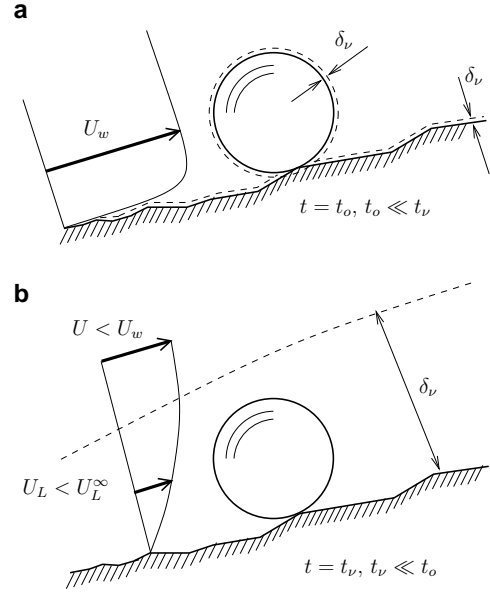


Figure 3: Sketches of the flow field around a pollen grain on an anther subject to a wind gust for (a) $\epsilon \gg 1$, and (b) $\epsilon \ll 1$.

strongly accelerated wind gusts $\epsilon \gg 1$. In this regime, the inertial time-variation of the outer flow dominates over the viscous effects, which occur on a much longer time scale. Since the Reynolds number of the pollen grain $\text{Re}_D = U_w D / \nu$ is not too large ($\text{Re}_D \sim 1.1 - 6.1$ for $U_w = 1\text{m/s}$), the drag force acting on the pollen grain may be calculated using the Stokes drag¹ $F_D = 3\pi\mu D U_w$ based on the free stream velocity, which yields a force range $F_D = 2.9U_w - 16.6U_w$ nN, where U_w is the wind velocity in m/s. The wind-gust explanation may then be appropriate to describe the release of relatively large pollen grains of diameters $D \gg (\nu t_o)^{1/2}$, for which $\epsilon \gg 1$, and adhesion forces in the range $2.9U_w - 16.6U_w$ nN, which corresponds to larger adhesion forces than those able to be overcome by steady wind conditions. Notice that, for the wind-gust time scale $t_o = 0.4\text{ms}$ (Aylor and Parlange, 1975), the critical diameter becomes $(\nu t_o)^{1/2} = 79.2\mu\text{m}$, which is larger than the diameters listed in Table 1 (with the exception of the maize pollen, which may be influenced by gravitational forces, as mentioned above).

Figure 3b shows a frozen sketch of the flow field around a pollen grain, after times of order t_v , for the more realistic $\epsilon \ll 1$ case for pollen shedding. After times of order t_v , the accelerating wind stream is not yet fully developed, and the boundary layer thickness has grown to be of the same size as the pollen grain diameter. The local velocity U_L is still smaller than its corresponding steady-state value (1), which is fully attained after times of order t_o . Time-dependent effects such as the added-mass and Basset forces (Kim and Karrila, 1993) may still be considered important effects at this point of the analysis, since these forces may be larger than the steady Stokes drag

¹Anther surface effects, which are important in a thin layer of thickness $\delta_v \sim \sqrt{\nu t_o}$, are neglected in the $\epsilon \gg 1$ regime since the velocity profile is nearly uniform on scales of order $D \gg \delta_v$.

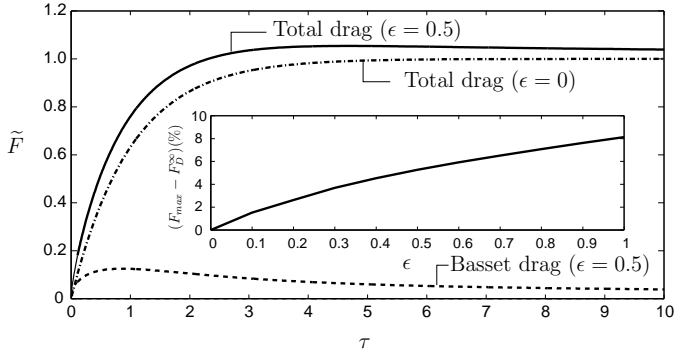


Figure 4: Total drag force and Basset forces for $\epsilon = 0$ and $\epsilon = 0.5$ calculated from (6). The added mass force is too small to distinguish at this scale. The inset shows the percentage variation of the maximum total drag force with respect to its steady value (2).

(2) during the transient regime $0 < t < t_v$ ². To address this question more rigorously, a local velocity variation of the form $\tilde{U} = 1 - \exp(-\tau)$ is considered, where \tilde{U} is the local velocity nondimensionalized with its steady-state value U_L^∞ given by (1) and τ is the time coordinate nondimensionalized with the gust time scale t_o . In this model, the boundary layer thickness grows progressively in time from an initial zero value. Since the local Reynolds number based on the grain radius $Re_D = U_L^\infty D/\nu$ is small, the unsteady hydrodynamic force can be estimated as (Kim and Karrila, 1993)

$$\begin{aligned} \tilde{F} &= c_1 \epsilon \frac{d\tilde{U}}{d\tau} + c_2 \epsilon^{1/2} \int_0^\tau \frac{d\tilde{U}}{d\xi} \frac{d\xi}{\sqrt{\tau - \xi}} + \tilde{U} \\ &= \tilde{F}_{AM} + \tilde{F}_B + \tilde{F}_D, \end{aligned} \quad (6)$$

with \tilde{F} the hydrodynamic force nondimensionalized with the steady Stokes drag force (2), and $c_1 = 1/(36 \cdot 1.7009)$ and $c_2 = 1/(2 \cdot 1.7009 \sqrt{\pi})$ are two geometric constants that result directly from such nondimensionalization. In this formulation, the three terms \tilde{F}_{AM} , \tilde{F}_B , and \tilde{F}_D denote the dimensionless added-mass, Basset, and Stokes drag forces respectively. It must be emphasized that equation (6) is an estimate of the unsteady force exerted on a sphere in a free stream: the effects of a nearby wall on the first two terms remain largely unknown. The relative values of each of the terms in (6) generally depend on time. In the asymptotic limit $\epsilon \ll 1$, three aerodynamic regimes of interest are found: $t \ll t_v \ll t_o$, $t \sim t_v \ll t_o$, and $t_v \ll t \sim t_o$, or equivalently, $\tau \ll \epsilon$, $\tau \sim \epsilon$ and $\tau \sim 1$.

For $\tau \ll \epsilon$ the flow around the pollen grain results in a nearly potential or irrotational flow (Lamb, 1945), except in very thin Stokes layers which grow on the solid surfaces. The dominant force at this stage is the added mass force $\tilde{F}_{AM} \sim \epsilon$, which is entirely produced by the inertia of the displaced fluid. The Basset force $\tilde{F}_B \sim (\epsilon\tau)^{1/2}$ and the Stokes force $\tilde{F}_D \sim \tau$ are in fact negligible at these short times, since $\tilde{F}_B/\tilde{F}_{AM} \sim (\tau/\epsilon)^{1/2} \ll 1$ and

$\tilde{F}_D/\tilde{F}_{AM} \sim \tau/\epsilon \ll 1$. For $\tau \sim \epsilon$ the boundary layer thickness, which grows as $(\tau/\epsilon)^{1/2}$, has reached a size sufficiently large to engulf the pollen grain. Once the boundary layer has grown sufficiently around the grain, it will detach, generating a recirculating flow that will start around the rear stagnation point. For $\tau \sim \epsilon$, the three terms in (6) are of order ϵ . For $\tau \sim 4\epsilon$, the Basset and Stokes drag are equal in the first approximation. Finally, for $\tau \sim 1$ and larger the flow is steady and fully viscous at scales of order D . The dominant force is then the steady Stokes drag force \tilde{F}_D that asymptotically reaches its steady value (2), with the added-mass and Basset forces exponentially small.

Figure 4 shows an example of the numerical integration of (6) for $\epsilon = 0$ and $\epsilon = 0.5$, which shows that, in the more physically realistic $\epsilon \ll 1$ regime for pollen shedding, the transient dynamics do not cause any significant force overshoot. The inset of Figure 4 shows the percentage variation of the maximum drag force with respect to (2) as a function of ϵ for $0 \leq \epsilon \leq 1$. As ϵ increases, the effects of the transient terms in (6) become more important, and transient forces slightly larger (within only a 10 % variation) than the Stokes drag F_D^∞ may occur. As ϵ increases, the wind-gust model used to calculate Fig. 4 misrepresents the magnitude of the velocity near the pollen grain, which becomes closer to U_w for large ϵ as observed in Fig. 3. These calculations show that the unsteady forces produce only a small overshoot in the total drag force on the pollen grain of at most an order of magnitude smaller than the steady Stokes drag force, reducing the significance of time-dependent effects in the boundary layer around the anther upon pollen release.

3. Aeroelastic shedding forces produced by atmospheric turbulence.

Atmospheric turbulence and its inherent unsteadiness may in fact play a notable role in pollen shedding, not in the sense of perturbing the viscous boundary layer near the anther surface as analyzed in Section 2.2 or previously conceptually proposed in earlier works (Aylor, 1975; Aylor and Parlange, 1975; Niklas, 1985; Jackson and Lyford, 1999; Aylor, 1999), but by promoting a shaking motion of the stamen. In this study, the energy flow from the oncoming fluid kinetic energy to the viscous drag forces on the pollen grain examined earlier (Aylor, 1975; Aylor and Parlange, 1975; Niklas, 1985; Jackson and Lyford, 1999; Aylor, 1999) is subtly modified, and thought of as an energy flow from the turbulent kinetic energy of the oncoming flow to the elastic energy of the stamen in the form of oscillating motion of the stamen, as depicted in Fig. 5. Finally, part of the kinetic energy is transferred to the pollen, which is ejected from the anther above a threshold mean wind speed. Aeroelasticity, the interaction between elastic structures and fluid flows (Simiu and Scanlan, 1996; Blevins, 1990), is a broad subject and has been used to examine the drag on trees (De Langre, 2008).

Since turbulence is inherently stochastic, it is appropriate to use a framework of mean displacements, velocities and accelerations, and fluctuations around these values. In particular, the longitudinal wind velocity is expressed as a sum of a mean velocity \tilde{U}_w and the velocity fluctuations around the mean $u'(t)$.

²It is worth noting that explanations of the effects produced by unsteady wind streams based on Rayleigh's problem (flat plate suddenly started from rest in a viscous fluid) used in earlier works on spore removal (Aylor, 1975; Aylor and Parlange, 1975), implicitly assume $t_o = 0$ (or $\epsilon \rightarrow \infty$) and are not appropriate in the $\epsilon \ll 1$ regime, since the time scale of acceleration is large compared with the viscous time scale.

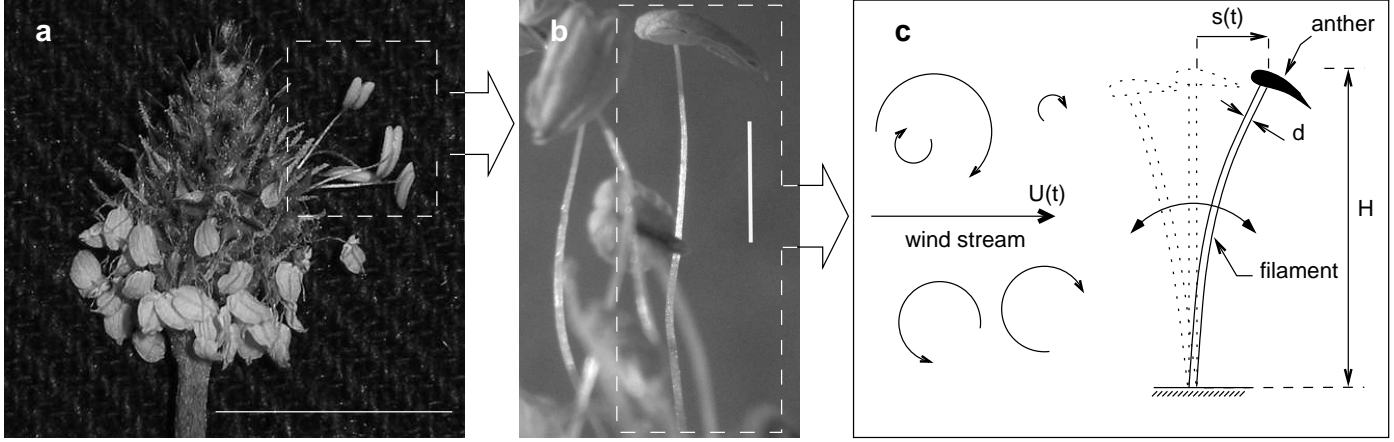


Figure 5: a) *Plantago* inflorescence (scale bar 1 cm) and b) anthers in scanning electron microscopy (scale bar 2 mm). Panel c) shows the mathematical model and aeroelastic motion schematics of a wind-pollinated stamen immersed in a turbulent wind stream of instantaneous velocity $U(t)$. Notice that the mathematical model has been reoriented in a horizontal position to enhance visualization.

The wind longitudinal velocity fluctuations are described by the power spectrum $E_u(\omega)$ that satisfies

$$\overline{u'^2(t)} = \int_0^\infty E_u(\omega) d\omega, \quad (7)$$

with ω the angular frequency. The power spectrum of the force and stamen acceleration fluctuations can be defined in a similar way to (7) by simply substituting the mean square of the corresponding fluctuation in the left hand side.

In what follows, the shedding process is thus no longer a deterministic process but a stochastic one. Pollen shedding conditions are expected to be determined by statistically extreme events, in the sense that the unsteady fluctuations of the force around a mean, steady value, are the interactions that may promote grains to dislodge; this happens when the induced aeroelastic forces on the stamen are larger than the threshold imposed by the pollen-anther molecular adhesion forces.

For simplicity we model the stamen as a linear isotropic elastic filament attached to a motionless substrate, with the center of pressure located in the anther as depicted in Fig. 5c. Elastic properties of the stamen can be obtained experimentally to yield the resonance frequency $\omega_n = (3EI/m_S H^3)^{1/2}$, where EI is the flexural rigidity, $m_S = m_a + m_f$ is the effective mass of the stamen and H is the filament length. The masses m_a and m_f denote the anther and filament mass respectively. For an elastic modulus $E \sim 100$ MPa, which corresponds to a typical stiffness of soft living vegetal tissues (De Langre, 2008), values of Table 1 yield a range $n = \omega_n/2\pi \sim 10.9 - 35.5$ Hz for the resonance frequency. Notice that these frequencies are much larger than characteristic natural frequencies of typical plant low-energy bulk motions, which are of the order of 1 Hz (Flesch and Grant, 1992; Doaré et al., 2004).

The system depicted in Fig. 5c corresponds to a linear damped oscillator, with the anther displacement $s(t)$ described by the stochastic ordinary differential equation

$$\ddot{s}(t) + 2\xi\omega_n\dot{s}(t) + \omega_n^2 s(t) = F(t)/m_S, \quad (8)$$

where $F(t)$ is the stochastic force exerted on the filament windward surface, which can be expressed as the sum of a mean force \bar{F} and force fluctuations around the mean $F'(t)$. In this formulation, ξ is the damping ratio caused by the viscous drag on the stamen during its motion relative to the mean flow and by structural dissipation in the plant material, and ω_n is the resonance frequency defined above. Typical values of ξ in plants and trees are of order $\xi \sim 0.1$ (Doaré et al., 2004; De Langre, 2008), which can be obtained by free oscillation tests (Flesch and Grant, 1992; Doaré et al., 2004). This coefficient may be much smaller for plant stamens because of the small dimensions and large resonance frequencies involved. An estimate of ξ can be obtained by assuming negligible structural dissipation in the plant material, so that only the hydrodynamic damping is present, with $\xi = \rho\bar{U}_w C_{De} A_e / (2\omega_n m_S)$ (Blevins, 1990), where C_{De} and A_e are respectively the effective drag coefficient and frontal area of the stamen structure. Additionally, the Reynolds numbers $Re_L = \bar{U}_w L/\nu$ and $Re_d = \bar{U}_w d/\nu$ are sufficiently small so that the damping ratio can be computed from the viscous drag on the anther. This is taken to be the sum of the drag on the anther head, modelled as a sphere of diameter L , and the drag on the filament, which is modelled as a slender tapering cylinder (Cox, 1970). The result is $\xi = \{4\pi\mu H / [\ln(2H/d) + 1/2] + 3\pi\mu L\} / \omega_n m_S$, which gives $\xi = 0.006 - 0.086$ for the species listed in Table 1. These values correspond to an underdamped system with free exponentially-decaying oscillatory behavior.

If the turbulent intensity squared is a small number, $T_u^2 = \overline{u'^2} / \bar{U}_w^2 \ll 1$, the force fluctuations may be linearized in the velocity fluctuations to give

$$F'(t) = \rho C_{De} A_e \bar{U}_w u'(t), \quad (9)$$

and the power spectrum of the force can be easily obtained from the power spectrum of the velocity fluctuations $E_u(\omega)$ by using (9) as thoroughly detailed in classical fluid-structure interaction texts (Simiu and Scanlan, 1996; Blevins, 1990). Turbulence intensity measurements in maize crops (Shaw et al., 1974), which

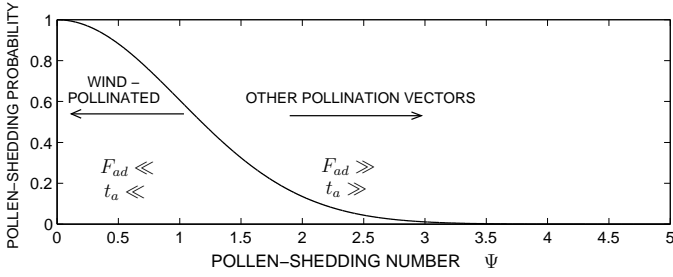


Figure 6: Pollen-shedding probability (12) as a function of the shedding number Ψ .

give an average of $T_u \sim 0.2 - 0.6$ depending on the height above the canopy, show that (9) is a good approximation.

By decomposing the anther acceleration $\ddot{s}(t)$ into the sum of a mean acceleration, which is of no interest because of its nonstochastic nature, and a fluctuation $\ddot{s}'(t)$, responsible for the stochastic inertial forces exerted on the pollen grain, a stochastic differential equation, similar to (8), can be obtained, which describes the time evolution of the fluctuation. The power spectrum of the acceleration fluctuations may be obtained from that of the longitudinal wind velocity fluctuations (Simiu and Scanlan, 1996; Blevins, 1990). The root-mean-square of the accelerations induced by the aeroelastic stamen motion on the pollen grain becomes $\sqrt{\ddot{s}'^2} = \bar{U}_w/t_a$, where t_a is a characteristic aeroelastic time given by

$$t_a = \left(\frac{\bar{U}_w}{2\xi\omega_n} \right) \left/ \left[\int_0^\infty \frac{\omega^4 E_u(\omega) d\omega}{|\mathcal{Z}(\omega)|^2} \right]^{1/2} \right., \quad (10)$$

where $|\mathcal{Z}(\omega)|^2 = (\omega_n^2 - \omega^2)^2 + 4\xi^2\omega^2\omega_n^2$ is the squared modulus of the impedance of the oscillatory system represented by equation (8). Non-unity aerodynamic admittance effects have been neglected in (10). An estimate of the aeroelastic time t_a can be calculated by integrating (10) using a von Kármán turbulent spectrum for the longitudinal velocity fluctuations,

$$E_u(\omega) = \frac{4u'^2\ell/\bar{U}_w}{\left[1 + 1.79 \left(\frac{\omega\ell}{\bar{U}_w} \right)^2 \right]^{5/6}}, \quad (11)$$

where ℓ is an integral length scale of the turbulent coarse vortices. The von Kármán spectrum has been widely used to analyze the turbulence-induced vibrations in man-made structures (Simiu and Scanlan, 1996; Blevins, 1990) and plants (Baker, 1995). Typical values $T_u = 0.5$ and $\ell = 1$ m for cereal crops (Baker, 1995) and estimates of ξ and ω_n mentioned above, based on Table 1, are used to numerically integrate (10), which gives $t_a = 0.14 - 0.26$ s at $\bar{U}_w = 1$ m/s, $t_a = 0.08 - 0.15$ s at $\bar{U}_w = 5$ m/s, and $t_a = 0.07 - 0.12$ s at $\bar{U}_w = 10$ m/s.

The critical fluctuating acceleration for pollen dislodgement \ddot{s}'_c of a single pollen grain is given by the value for which the inertial aeroelastic forces are of the same order of magnitude as the adhesion force F_{ad} , so that $\ddot{s}'_c = F_{ad}/m_p$.

In this stochastic framework, the anther displacement fluctuation $s'(t)$ and its time-derivatives are described by an associated probability density function (PDF), obtained by solving

the associated Fokker-Planck equation to equation (9). Since the dissipation ξ is relatively small in this system, the majority of the response of the stamen to the turbulent flow may occur in a narrow band of frequencies centered about the natural frequency ω_n . For simplicity, the probability density function is assumed to be a Rayleigh distribution in the first approximation, which represents a narrow-band Gaussian random process (Blevins, 1990). Such distribution yields the *probability of pollen shedding*,

$$P(\ddot{s}' > \ddot{s}'_c) = e^{-\Psi^2/2}, \quad (12)$$

where

$$\Psi = \frac{\ddot{s}'_c}{\sqrt{\ddot{s}'^2}} = \frac{F_{ad}t_a}{\bar{U}_w m_p}, \quad (13)$$

is a *pollen-shedding number*.

Equation (12) represents the probability of pollen shedding by aeroelastic forces $P(\Psi)$, as shown in Fig. 6, in terms of a single nondimensional parameter or shedding number Ψ given by equation (13), that may be thought of as a quantity proportional to the ratio of the adhesion force F_{ad} to the root-mean-square of the characteristic aeroelastic force fluctuations exerted on the pollen grain $m_p\bar{U}_w/t_a$. Typical wind-pollinated species are then expected to release pollen grains over small aeroelastic time scales and to have small adhesion forces, with $\Psi \ll 1$ a small number. The opposite trend would hold for species pollinated by other vectors. Values of acceleration greater than six times the root-mean-square acceleration \bar{U}_w/t_a are very unlikely to be observed in turbulence-induced vibrations that follow the cumulative probability distribution (12) (Blevins, 1990). Therefore, $\Psi \leq 6$, or equivalently, the force of adhesion F_{ad} may have to yield a value $F_{ad} \leq F_{ad}^* = 6\bar{U}_w m_p/t_a$ for the aeroelastic mechanism to represent a suitable description of wind-pollination. Based on pollen mass values given in Table 1 and estimates of t_a mentioned above, the range of values of the maximum allowed adhesion force are $F_{ad}^* \sim 0.6$ nN at a wind velocity $\bar{U}_w = 1$ m/s, $F_{ad}^* \sim 5$ nN at $\bar{U}_w = 5$ m/s, and $F_{ad}^* \sim 13$ nN at $\bar{U}_w = 10$ m/s. According to the simplified stamen model analyzed in this investigation, the stamen acceleration produced by the aeroelastic forces is sufficiently large to dislodge the pollen grains if the pollen-anther adhesion force is smaller than F_{ad}^* at the corresponding wind velocity. It is worth noting that the values of F_{ad}^* are physically feasible in anemophilous species and comparable to the range of adhesion forces that are able to be overcome by purely steady aerodynamic forces. Nonetheless, more accurate evaluation of Ψ requires the experimental determination of F_{ad} and calculation of t_a , which requires accurate experimental determination of $C_{De}A_e$ or ξ , and E or ω_n for each species.

4. Conclusions.

Earlier attempts to solve the paradox of pollen liberation, based on wind-gust aerodynamic models of unsteady viscous forces exerted on a fungal spore attached to a motionless substrate in a boundary layer, are shown in this study to be inappropriate to describe pollen shedding. Steady Stokes drag forces

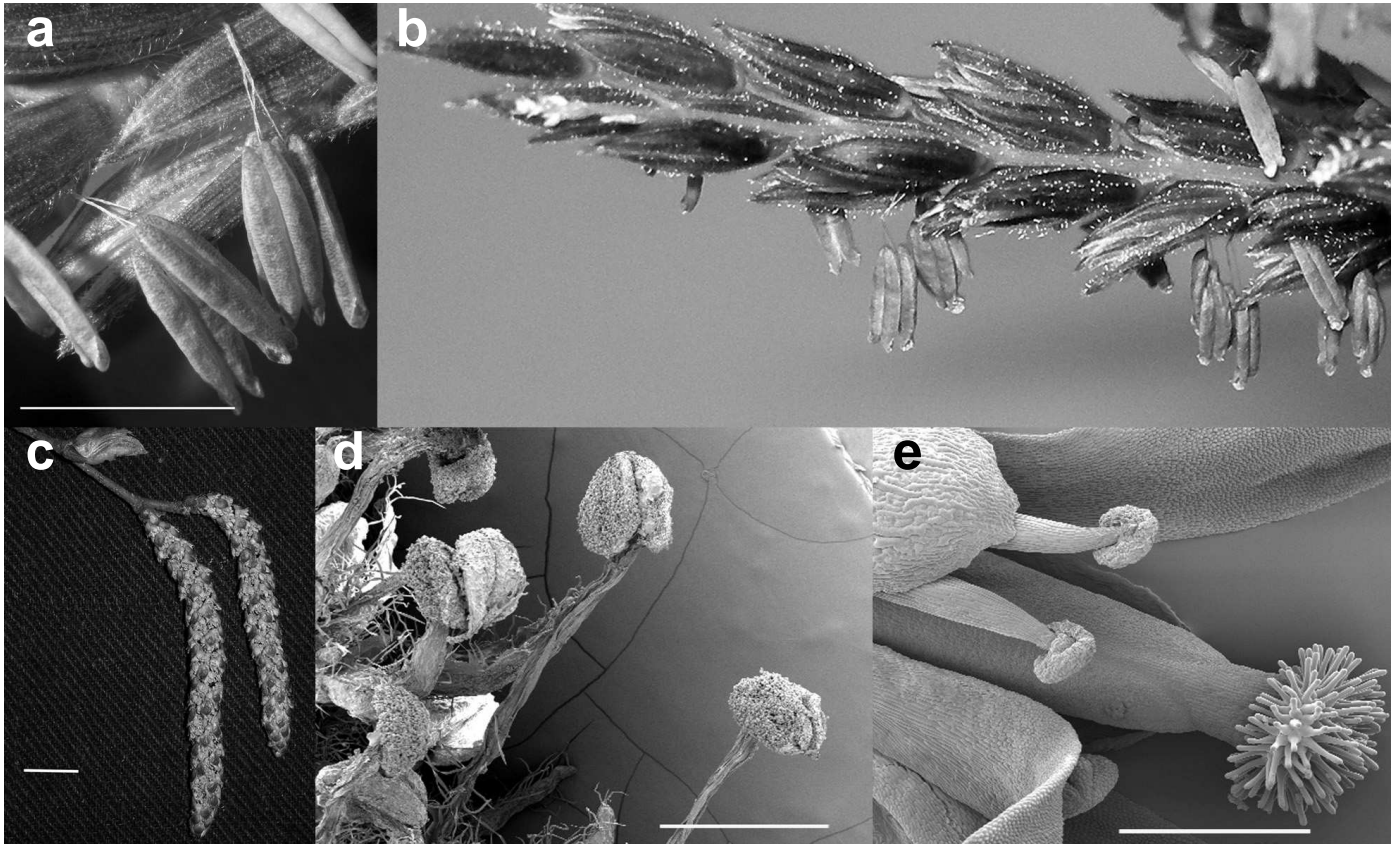


Figure 7: a) *Zea mays* anthers (scale bar, 5 mm) and b) inflorescence; c) *Betula albosinensis* catkin (scale bar, 1 cm), d) *Salix sepulchralis* anthers (scanning electron microscopy; scale bar, 1 mm); e) In contrast, self-fertile *Arabidopsis thaliana* anthers have shorter, less mobile filaments (scanning electron microscopy; scale bar, 500 μm).

are found to be capable of removing pollen from anemophilous anthers. Since viscous effects are found to be more important in typical anemophilous pollen than inertial accelerations of the outer wind stream, with the ratio ϵ of the viscous time scale t_v to the wind-gust time scale t_o typically a small number, unsteady boundary-layer forces produced by wind gusts are found to be mostly ineffective. Nonetheless, removal of pollen by wind gusts may occur for sufficiently large pollen grains.

We have proposed a new turbulence-initiated, wind-pollination mechanism to explain the phenomenon in a complementary way. A straightforward scaling analysis, accounting for the level of turbulence near the ground and the elastic properties of the plant, gives a first approximation of the quantitative probabilistic measure of pollen shedding when the anthers are shaken by the stochastic action of the wind. The effectiveness of this mechanism depends on the shedding number $\Psi = F_{ad} t_a / m_p \bar{U}_w$, which is found to be an order-unity parameter when estimated from typical turbulent power spectra. Nonetheless, a more accurate evaluation of the shedding number needs an accurate determination of the pollen-anther adhesion force and aeroelastic times, two magnitudes that are difficult to define experimentally and therefore unexplored in the existing literature. Further analyses on more elaborated aeroelastic models, and their experimental validation, accounting for a wider range of biomechanical effects, such as a plant physical

representation by a structure with multiple degrees of freedom and non-uniform mechanical properties, will allow a fuller understanding of the processes involved in the shedding of pollen.

We note that not all wind-pollinated plants have such long anthers. However, where anther filaments are short or solid, it is invariably the case that wind-pollinated flowers are borne on mobile, flexible inflorescence stems (catkins; Fig. 7), or, in the case of gymnosperm anthers, the male cones are borne on long, flexible branches. These different mechanical solutions to the same problem represent independent evolutionary innovations, but all may operate within the simple model we describe here.

One of the most important features of a suitable long-range dispersal model of pollen grains or fungal spores is the characterization of the physical and biological processes that occur in the source and release of these small particles into the air. The extraordinary model sensitivity to these small-scale processes sets pollen-transport models apart from pure pollutant dispersal models, where the source is reasonably independent of the surrounding micrometeorology.

These models may inform future analysis of pollen dispersal for crop production, maintenance of biodiversity, and management of genetically modified plants.

Acknowledgments

This work was funded by HFSP grant RGY0073/2005-C to B.J.G. and S.G.L.S. The first author is grateful to Dr. V. Morin for interesting discussions on the subject.

A. Appendix: Microscopy and measurements.

Representative measurements were made for a range of wind-pollinated, or partially wind-pollinated, species for as many of the characteristics listed (Table 1) as possible. Supplementary data was taken from the literature where available. To measure pollen dimensions, and where anther filaments could not be measured without microscopy, fresh plant material was collected at the Cambridge University Botanic Gardens (Cambridge, UK) and immediately frozen in liquid nitrogen. Following freeze drying and sputter coating with gold, measurements were made (Scion Image; Scion Corp, Frederick, Maryland, USA) on digital images recorded using scanning electron microscopy (Oxford Instruments CT 1500; Abingdon, Oxfordshire, UK).

References

- Aylor, D.E. (1985) Force required to detach conidia of *Helminthosporium maydis*. *Plant Physiol.* 55, 99-101.
- Aylor, D.E. (1999) The role of intermittent wind in the dispersal of fungal pathogens. *Annu. Rev. Phytopat.* 28, 73-92.
- Aylor, D.E., Parlange, J.Y. (1975) Ventilation required to entrain small particles from leaves. *Plant Physiol.* 56, 97-99.
- Baker, C.J. (1995) The development of a theoretical model for the windthrow of plants. *J. Theor. Biol.* 175, 355-372.
- Blevins, R.D. (1990) Flow-induced vibration. Van Nostrand Reinhold, New York.
- Crane, P.E., Friis, E.M, Pedersen, K.R., (1995) The origin and early diversification of angiosperms. *Nature* 374, 23-33.
- Connor, H.E. (1990) Breeding systems in New Zealand grasses. XI. Gynodioecism in *Chionochloa bromoides*. *New Zealand J. Bot.* 28, 59-65.
- Cox, R.G. (1970) The motion of slender bodies in a viscous fluid. Part 1: General theory. *J. Fluid Mech.* 44, 791-810.
- De Langre, E. (2008) Effects of wind on plants. *Annu. Rev. Fluid Mech.* 40, 141-168.
- Doaré, O., Moullia, B., De Langre, E. (2004) Effect of plant interaction on wind-induced crop motion. *J. Biomech. Eng.* 126, 146-151.
- Emberlin, J., Adams-Groom, B., Tidmarsh, J. (1999) A Report on the Dispersal of Maize Pollen. Commissioned by the Soil Association. Worcester University College, Worcester.
- Finnigan, J. (2000) Turbulence in plant canopies. *Annu. Rev. Fluid Mech.* 32, 519-571.
- Flesch, T.K., Grant, R.H. (1992) Corn motion in the wind during senescence: effect of dynamic plant characteristics. *Agron. J.* 84, 742-747.
- Golonka, A.M., Sakai, A.K., Weller, S. G. (2005) Wind pollination, sexual dimorphism, and changes in floral traits of Schiedea (*Caryophyllaceae*). *Am. J. Bot.* 92, 1492-1502.
- Hammer, K. (2005) Remarks to the breeding systems of the *Triticeae* with special reference to the pollen to ovule ratios. *Czech J. Genet. Plant Breed* 41, 145-153.
- Jackson, S.T., Lyford, M.E., (1999) Pollen dispersal models in quaternary plant ecology: assumptions, parameters and prescriptions. *Botanical Rev.* 65, 39-75.
- Kim, S., Karrila S.J. (1993) *Microhydrodynamics*. Dover, New York.
- King, M.J., Lengoc, L. (1993) Vibratory pollen collection dynamics. *T. ASAE* 36, 135-140.
- King, M.J., Buchmann, S.L. (1995) Bumble-bee initiated vibration release mechanism of *Rhododendron* pollen. *Am. J. Bot.* 82, 1407-1411.
- Komaki, M.K., Tsunewaki, K. (1981) Genetical studies on the difference of anther length among common wheat cultivars. *Euphytica.* 30, 45-53. 7.
- Lamb, H. (1945) *Hydrodynamics*. Dover, New York.
- Niklas, K.J. (1985) Aerodynamics of wind pollination. *Botanical Rev.* 51, 328-386.
- O'Neill, M.E. (1968) A sphere in contact with a plane wall in a slow linear shear flow. *Chem. Eng. Sci.* 23, 1293-1298.
- Schlichting, H. (1979) *Boundary layer theory*. McGraw-Hill, New York.
- Sharma, N., Koul, P., Koul, A.K. (1992) Reproductive biology of *Plantago*: shift from cross- to self-pollination. *Ann. Bot.* 69, 7-11.
- Shaw, R.H., Den Hartog, G., King, K.M., Thurtell, G.W. (1974) Measurements of mean wind flow and three-dimensional turbulence intensity within a mature corn canopy. *Agric. Meteor.* 13, 419-425.
- Simiu, E., Scanlan, R.H. (1996) *Wind effects on structures*. John Wiley, New York.
- Willis, K.J., McElwain, J.C., (2002) *The Evolution of Plants* (Oxford University Press, Oxford).

Table 1: Representative measurements of anthers, filaments and pollen from a range of wind or partially wind-pollinated species.

Species	Anther mass m_a (mg)	Anther length L (mm)	Filament+ anther mass m_s (mg)	Filament length H (mm)	Filament diameter d (mm)	Pollen mass m_p (ng)	Pollen diameter D (μm)	Viscous-gust time scale ratio $\epsilon = t_v/t_o$
<i>Betula coerulograndis</i> (birch)		0.83		0.51**	0.18**		25.30	0.10
<i>Betula albosinensis</i> Hergest (birch)		0.69					24.47	0.09
<i>Briza</i> sp. (grass)		2.99					23.45	0.08
<i>Chionocloa bromoides</i> (grass)		3.41 ⁽¹⁾						
<i>Pinus sylvestris</i> (pine)						21.95 ⁽⁵⁾	59.00 ⁽⁵⁾	0.55
<i>Plantago lanceolata</i> (plantain)	0.08	2.11	0.11	7.2	0.06	14.40 ⁽⁵⁾	29.75	0.14
<i>Plantago ovata</i> (plantain)		0.60 ⁽²⁾						
<i>Salix caprea</i> * (willow)	0.07	0.66	0.28	9.63	0.10	3.43 ⁽⁵⁾	16.68	0.04
<i>Salix sepulcralis</i> var <i>chrysocoma</i> * (willow)	0.09	0.56	0.25	5.58	0.11		19.76	0.06
<i>Schiedea</i> sp. (Hawaiian shrub)		4.25 ⁽³⁾						
<i>Thalictrum polycarpum</i> (meadow rue)		1.74		3.05	0.10		23.37	0.08
<i>Trictium aestivum</i> (wheat)		2.85 ⁽⁴⁾					51.8 ⁽⁶⁾	0.42
<i>Zea mays</i> (maize)				3.92		219-380	95.29	1.44

*Members of the genus *Salix* are reported to be part-insect, part wind-pollinated.

***Betula* catkins contain shorter, wider anther filaments.

References: ⁽¹⁾Connor (1990), ⁽²⁾Sharma et al. (1992), ⁽³⁾Golonka et al. (2005), ⁽⁴⁾Komaki and Tsunewaki (1981), ⁽⁵⁾Jackson and Lyford (1999),

⁽⁶⁾Hammer (2005).